Palaeogeography, Palaeoclimatology, Palaeoecology 655 (2024) 112553

Contents lists available at ScienceDirect

Palaeogeography, Palaeoclimatology, Palaeoecology

journal homepage: www.elsevier.com/locate/palaeo

Modern reconstructions of mean and seasonal-scale climate from coastal marine gastropods (Turritellidae)

Serena R. Scholz [a,b,*], Sierra V. Petersen [b], Brendan M. Anderson [c]

[a] Yale University, Department of Earth and Planetary Sciences, 210 Whitney Ave., New Haven, CT 06511, USA
[b] University of Michigan, Earth & Environmental Sciences Dept, 1100 North University Ave., Ann Arbor, MI 48109, USA
[c] Paleontological Research Institution, 1259 Trumansburg Rd, Ithaca, NY 14850, USA

ARTICLE INFO

Editor: M Elliot

Keywords:
Oxygen isotopes
Sclerochronology
Modern calibration
Seasonal climate
Turritellidae
Gastropods

ABSTRACT

Turritellid gastropods are aragonitic marine mollusks that are particularly abundant and widespread in the fossil record. With fast growth rates and a shallow coastal habitat, the oxygen isotopic composition of their shells has the potential to be an excellent recorder of ancient subannual climate variation. To date, tests of the reliability of oxygen isotope paleothermometry in this family of gastropods have been restricted to a few localities. We produce 15 new high-resolution oxygen isotope profiles of modern turritellid shells, and combine these with 28 other published profiles from a range of latitudes and locations in order to investigate generalizable relationships between shell $\delta^{18}O_{carb}$ and local climate data including temperature, precipitation, salinity, and $\delta^{18}O_{sw}$. We find that turritellids accurately record mean SST values using existing temperature-$\delta^{18}O_{carb}$ relationships, but seasonal ranges in SST are frequently overestimated. Modern climate data from our study sites show correlations that can explain this overestimation through the following proposed mechanism: seasonal increases/decreases in rainfall lead to decreases/increases in local salinity and, by inference, $\delta^{18}O_{sw}$, amplifying the seasonal signal in $\delta^{18}O_{carb}$. We find that ignoring these seasonal variations in $\delta^{18}O_{sw}$ can significantly bias the calculation of seasonal temperature ranges from $\delta^{18}O_{carb}$ profiles derived from turritellids. Similar processes may also affect sclerochronological records from other nearshore, shallow-water marine calcifiers.

1. Introduction

The seasonal cycle is an important component of climate variability, particularly for constraining the geographic distribution of flora and fauna. Biota are often more affected by seasonal extremes than by changes in mean annual temperature (MAT) or mean annual precipitation (MAP). However, changes in the seasonal cycles throughout time can be difficult to reconstruct due to time-averaging in many paleoclimate archive materials. Beyond temperature, reconstructing changes in the subannual hydrological cycle is particularly difficult due to a lack of suitable archives.

The isotopic composition of mollusk shells can provide subannual environmental data about their habitat, allowing reconstruction of past seasonality (De Winter et al., 2020). The $\delta^{18}O$ of shell carbonate ($\delta^{18}O_{carb}$) is controlled by two factors: the temperature, and the isotopic composition of the water the shell grew in (seawater for marine taxa, $\delta^{18}O_{sw}$) (Grossman and Ku, 1986; Kim et al., 2007; Grossman, 2012). In order to obtain temperature estimates, many studies assume that $\delta^{18}O_{sw}$ is constant throughout the year, allowing it to be neglected in calculations of seasonal range. This is a reasonable assumption in deeper shelf environments, which don't experience much seasonal variability in salinity, or, by assumption, in $\delta^{18}O_{sw}$. However, in shallower-water regimes (e.g., Ivany et al., 2008; Huyghe et al., 2015; Crippa et al., 2016), spatial and temporal variation in $\delta^{18}O_{sw}$ can occur. These variations may be due to above-ground freshwater or submarine groundwater discharge (Dettman et al., 2004; Zhang et al., 2021), lateral or vertical advection of water masses with different $\delta^{18}O_{sw}$ values (Tao et al., 2013), or seasonally variable freshwater runoff driven by periods of heavy precipitation, which could lead to seasonal changes in $\delta^{18}O_{sw}$ in near-shore waters. Neglecting these seasonal changes in $\delta^{18}O_{sw}$ could significantly bias seasonal temperature estimates deriving from mollusks that live in these shallower, nearshore regimes.

Many previous isotope-based paleoclimate studies have focused on long-lived bivalves due to their ability to produce decades-long records, but their slow growth rates can result in annual growth bands that are 1 mm in width or less (Buick and Ivany, 2004; Ivany, 2012), requiring

* Corresponding author at: Yale University, Department of Earth and Planetary Sciences, 210 Whitney Ave., New Haven, CT 06511, USA.
E-mail address: serena.scholz@yale.edu (S.R. Scholz).

https://doi.org/10.1016/j.palaeo.2024.112553
Received 25 February 2024; Received in revised form 26 August 2024; Accepted 8 October 2024
Available online 10 October 2024

micro-drilling techniques to sample material at a sub-yearly scale. In contrast, many gastropods are faster growing, enabling sub-annual sampling with ease using a hand-held drill (e.g. Jones and Allmon, 1995; De Winter et al., 2020; Scholz et al., 2020). The rapid growth rate also allows for collection of larger quantities of carbonate powder while maintaining sub-annual resolution – an important feature necessary for certain techniques that can require more material, such as clumped isotope paleothermometry (Huntington and Petersen, 2023).

Turritellid gastropods (Cerithioidea: family Turritellidae) are extremely abundant and widespread in the fossil record, occurring on all continents and commonly in marine deposit since the Early Cretaceous (Allmon, 2011). Turritellids are nearly all semi-infaunal suspension feeders, with some known to deposit feed (Allmon, 2011). They predominately inhabit shallow water environments (10–100 m), but individual species are known to inhabit both very shallow (<5 m) and deep water environments (>500 m, e.g., *Colpospira curialis*, *Turritella yucatecana*) (Allmon, 1988, 2011). It is possible that some species may be present at a range of depths, either seasonally or because of broad bathymetric tolerances. *Maoricolpus roseus* is typically found in shallow waters, but is known to occur alive at depths from the intertidal to more than 200 m (Gunaskera et al., 2005). Allmon (1988, 2011) and Waite and Allmon (2016) have suggested that it is likely some species may migrate seasonally between habitats of different water depths, but this has not been verified observationally and is unlikely to represent extreme bathymetric variability.

Turritellids typically inhabit fully marine salinities, but some species can tolerate brackish water, especially near the mouths of large rivers, with *Turritellinella tricarinata* tolerating salinities as low as 18–24 psu (Avens and Sleigh, 1965; Shumway, 1979), *Turritella (s.l.) annulata* occurring in coastal lagoons with salinities as low as 12–15 psu (Blay and Dongdem, 1996), and *Turritella bacillum* observed to tolerate salinities as low as 10–15 psu (Shin et al., 2020). High abundances of turritellids in both the fossil record and modern environments are commonly associated with nutrient rich environments, with nutrients supplied either by local upwelling or terrestrial runoff (Allmon, 1988, 2007; Jones and Allmon, 1995; Anderson et al., 2017; Shin et al., 2020; Scholz et al., 2020).

Turritellid shells have previously been used for stable-isotope-based environment and seasonality reconstructions (Allmon et al., 1992, 1994; Jones and Allmon, 1995; Andreasson and Schmitz, 1996, 1998, 2000; Teusch et al., 2002; Waite and Allmon, 2013, 2016; Kwan et al., 2018; Shin et al., 2020; Scholz et al., 2020). They grow rapidly during their juvenile stage, with the largest species depositing up to 35 g of carbonate in the first year of life (Anderson and Allmon, 2020), making them especially appealing taxa for subannual studies. The sinusoidal nature of turritellid $\delta^{18}O_{carb}$ profiles suggest that they can be excellent recorders of paleoseasonality, without the significant seasonal biases due to stoppages of growth seen in other taxa (e.g. Surge et al., 2001).

In order to accurately use turritellid oxygen isotope profiles to reconstruct paleoseasonality, it is essential to first validate how turritellids record seasonal climate cycles in a modern context, where detailed climate data exist for comparison. Modern calibration studies of turritellids have been previously performed by Allmon et al. (1992) and Teusch et al. (2002), using specimens collected in Mexico and Chile. By assuming $\delta^{18}O_{sw}$ was constant throughout the year, these studies found that subannual range in $\delta^{18}O_{carb}$ accurately reconstructed the observed average summertime, wintertime, and annual range in sea surface temperature (SST). However, these studies focus only on a single location and species each. Here, we present new subannual-scale isotope profiles from shells of modern turritellids, sourced from a variety of latitudes and belonging to many different species, in order to study generalizable relationships between shell $\delta^{18}O_{carb}$ values and local climate data including temperature, salinity, precipitation, and $\delta^{18}O_{sw}$. We show that while turritellids can provide good estimates of mean sea surface temperatures, ignoring seasonal variations in $\delta^{18}O_{sw}$ can significantly bias the calculation of seasonal temperature ranges in sites with significant seasonal variation in precipitation and salinity.

2. Methods

2.1. Shells and species

15 turritellid shells representing seven different species, *Turritellinella tricarinata* (Brocchi, 1814; the senior synonym of *Turritella communis* Risso, 1826–see Harzhauser and Landau, 2019), *Turritella (s.s.) terebra* (Linnaeus, 1758), *Caviturritella leucostoma* (Valenciennes, 1832), *Turritella (s.l.) carinifera* Lamarck, 1822, *Turritella (s.s.) bacillum* (Kiener, 1843), *Turritella (s.l.) bicingulata* (Lamarck, 1822),and *Turritella duplicata* (Linnaeus, 1758), were obtained from the University of Michigan Zoology Collections. These shells were collected from 9 locations worldwide: Mexico (Acapulco & Puerto Penasco), Costa Rica, the Philippines, South Africa, India, Sri Lanka, Cape Verde and England (Table S1, Fig. 1, open circles). In addition to these 15 shells, published isotopic data from 28 additional shells was included to expand the dataset (Allmon et al., 1992, 1994; Teusch et al., 2002; Waite and Allmon, 2013, 2016; Kwan et al., 2018; Shin et al., 2020; Scholz et al., 2020). These included four additional turritellid species: *Caviturritella gonostoma* (Valenciennes, 1832), *C. variegata* (Linnaeus, 1758), *Incatella cingulata* (G. B. Sowerby I, 1825), and *Maoricolpus roseus* (Quoy & Gaimard, 1834), and 9 additional locations (New Zealand, Chile, Mexico (San Felipe), Tasmania, Thailand, Hong Kong, Jamaica, Venezuela, and Colombia) (Fig. 1, crosses). These sites cover six continents and a latitude range of 47°S to 50°N, thus representing a wide range of environments and species. Locations and species are described in Table 1.

Specificity of shell collection location and date of collection available from newly studied museum specimens varied from a specific beach ("Playa Avellana, Costa Rica") to a whole country ("Cape Verde"). Shells were collected dead on the beach and were inferred to reflect modern climate from that site, though exact collection dates are not known for all specimens (see 2.3. Climate parameters).

2.2. Drilling and isotope measurements

Shells were sampled with a hand drill at subannual resolution along the spiral growth direction, with samples taken equidistant from the sutures between whorls (Fig. S1). Accumulated spiral distance (in mm) was recorded starting at 0 near the apex and increasing towards the aperture. Samples were taken from the top 1 mm of the shell surface to exclude inclusion of internal material that may have been deposited at a different time than initial exterior shell growth. 12–47 samples were taken per shell, depending on shell size, with most shells having 20–30 samples. Samples were spaced ~3-10 mm apart, depending on shell size, similar to previous turritellid studies. Carbonate powders were analyzed at the University of Michigan Stable Isotope Facility for $\delta^{13}C_{carb}$ and $\delta^{18}O_{carb}$, using a Kiel IV device attached to a Thermo-MAT 253 mass spectrometer and calibrated against NBS-19 and NBS-18, run daily. Analytical error was better than ±0.1 ‰ for both $\delta^{13}C_{carb}$ and $\delta^{18}O_{carb}$. All $\delta^{13}C_{carb}$ and $\delta^{18}O_{carb}$ data are presented relative to Vienna Pee Dee Belemnite (VPDB).

Mollusks may preferentially grow in one season, with differences in seasonal biases between taxa dependent on the taxa's thermal tolerances and the local climate. With a fixed sampling resolution, this means the mean of all $\delta^{18}O_{carb}$ points may be weighted towards the season of more rapid growth, given sufficient seasonal growth rate differences. Therefore, in addition to the mean, the midpoint of $\delta^{18}O_{carb}$ in each shell profile (the halfway point between the minimum and maximum measured values in each profile) was calculated in order to detect any seasonal biases in $\delta^{18}O_{carb}$ data. The midpoint should provide a more accurate reflection of average conditions than the mean in the case that the shell grew unequally throughout the year. If shell growth was constant throughout the year, the mean and midpoint should be equal. Midpoints (as well as means) may still be skewed from true average

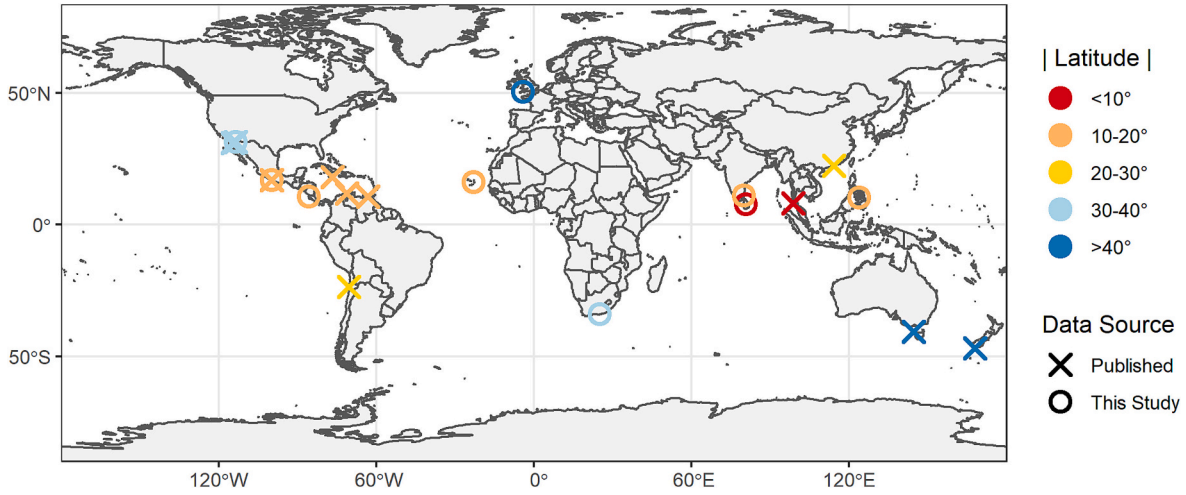

Fig. 1. Locations of new samples from this study (open circles) and previously-published samples (crosses), colored by absolute value of latitude. Published values come from Allmon et al., 1992, 1994; Teusch et al., 2002; Waite and Allmon, 2013, 2016; Kwan et al., 2018; Shin et al., 2020; Scholz et al., 2020.

Table 1
Locations and species used in this study, and previously published studies. Individual specimen information can be found in supplementary information, Table S1.

Location	Species - number of specimens	Source
Cape Verde	*Turritella (s.l.) bicingulata - 2*	This study
Antofagasta, Chile	*Incatella cingulata - 2*	Teusch et al., 2002
Guajira Peninsula, Colombia	*Caviturritella variegata – 2*	Scholz et al., 2020
Playa Avellana, Costa Rica	*Caviturritella leucostoma - 2*	This study
Plymouth Harbor, England	*Turritellinella tricarinata - 2*	This study
Hong Kong	*Turritella s.s. bacillum – 4*	Kwan et al., 2018
	Turritella s.s. bacillum – 4	Shin et al., 2020
Tharamgambadi, India	*Turritella (Zaria) duplicata - 2*	This study
Jamaica	*Caviturritella variegata – 2*	Scholz et al., 2020
Stewart Island, New Zealand	*Maoricolpus roseus – 1*	Allmon et al., 1994
Acapulco, Mexico	*Caviturritella leucostoma – 1*	This study
	Caviturritella gonostoma - 1	Scholz et al., 2020
Puerto Penasco, Mexico	*Caviturritella leucostoma – 2*	This study
	Caviturritella gonostoma - 3	Allmon et al., 1992
	Caviturritella leucostoma – 1	Waite and Allmon, 2013
San Felipe, Mexico	*Caviturritella leucostoma - 2*	Waite and Allmon, 2013
Cebu City, Philippines	*Turritella (s.s.) terebra – 1*	This study
Jeffreys Bay, South Africa	*Turritella (s.l.) carinifera – 1*	This study
Sri Lanka	*Turritella (s.s.) bacillum – 2*	This study
Cape Grim, Tasmania	*Maoricolpus roseus – 2*	Allmon et al., 1994
Phang Nga Bay, Thailand	*Turritella (Zaria) duplicata – 3*	Waite and Allmon, 2016
Carupano, Venezuela	*Caviturritella variegata - 2*	Scholz et al., 2020

conditions if an entire season is completely excluded from a profile through growth cessation. The short lifespan of turritellids and sinusoidal nature of their $\delta^{18}O_{carb}$ profiles allow us to take the simple approach of means vs. midpoints to assess growth biases. However, in cases where precise estimates of lifespan and growth rates are needed, where there is reason to believe significant seasonal cessations of growth occur, or for long-lived taxa, more advanced techniques for addressing growth biases may be necessary (Judd et al., 2018; Ivany and Judd, 2022).

Mollusk lifespan was determined by identifying multi-point extrema in a given $\delta^{18}O_{carb}$ profile and assuming alternating extrema corresponded to summers and winters. Previous work has shown there is no clear correspondence between visible growth lines and sclerochronologically-derived lifespans in most gastropods, including turritellids (Allmon, 2011; De Winter et al., 2020), so growth lines were not incorporated in lifespan estimates.

2.3. Climate parameters

Monthly average sea surface temperature (SST) data for each sample location were calculated from NOAA ERSST v.5 reanalysis (Huang et al., 2017), which has temperatures derived from the International Comprehensive Ocean–Atmosphere Dataset. Monthly average salinity was calculated using the SODA v.3.3.1 reanalysis product (Carton et al., 2018), and monthly average precipitation data were calculated from the CRU 3.25 Global Precipitation dataset (Harris et al., 2014). All monthly data were averaged over the period 1980–2012 for a rectangular spatial region ($2^\circ \times 2^\circ$) around the sample location (Table S2). Annual ranges in SST (ART), salinity (ARS), and precipitation (ARP) were calculated for all sites by taking the difference between the maximum and minimum monthly average value (Fig. 2). Mean annual sea surface temperature (MASST) and mean annual salinity (MAS) were determined by taking the average of all monthly means, and mean annual precipitation (MAP) was calculated as the sum of the monthly means. To compare timing of maximum seasonal SST, salinity, and precipitation, cross correlation functions were performed for all sites, with a maximum lag of 12 months (Fig. S2). Because the exact collection age of museum specimens was uncertain, we repeated some of our analyses using preindustrial SST data (1890–1910) for museum specimens with unknown collection dates. This did not alter any of the conclusions stated below (Fig. S3). All figures present temperature data from the 1980–2012 interval.

In order to calculate SST from shell $\delta^{18}O_{carb}$, we obtained average $\delta^{18}O_{sw}$ values from all locations from LeGrande and Schmidt (2006), a gridded interpolation based on data from the Global Seawater Oxygen-18 Database from NASA GISS (Schmidt et al., 1999, Fig. 3d). For comparison to the $\delta^{18}O_{sw}$ obtained from LeGrande and Schmidt (2006), we also calculate $\delta^{18}O_{sw}$ based on the empirical relationship between mean annual salinity (MAS) and $\delta^{18}O_{sw}$ presented in Brennan et al. (2012):

$$\delta^{18}O_{sw} = 0.55MAS–19.1$$

2.4. Calculating temperature from $\delta^{18}O_{carb}$

Using the value of $\delta^{18}O_{sw}$ at each sample location and a selected $\delta^{18}O$ value from a given shell, we calculated a corresponding temperature according to the equation for mollusks (primarily based on gastropods) presented in Grossman (2012) where:

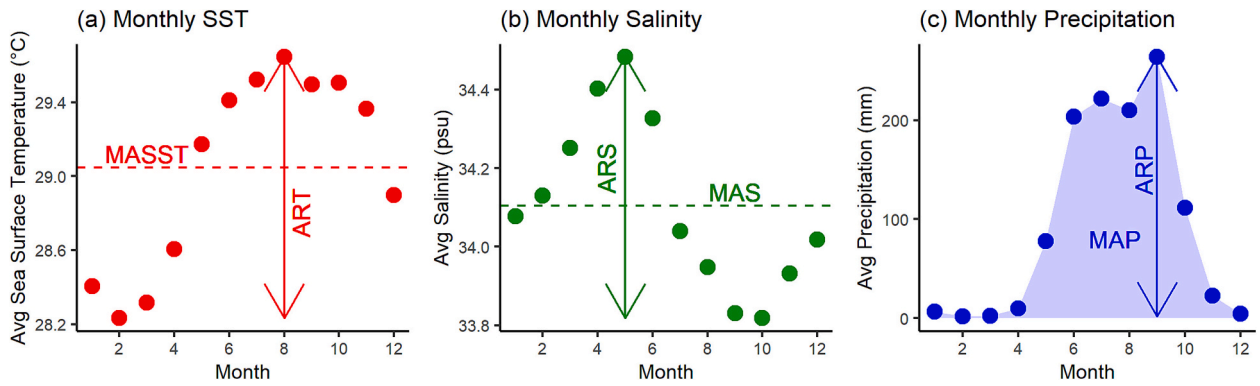

Fig. 2. Annual climatological profiles for an example location (Acapulco, Mexico) for monthly (a) SSTs, (b) salinity, and (c) precipitation. Dashed lines in (a) and (b) show Mean Annual Sea Surface Temperature (MASST) and Mean Annual Salinity (MAS), respectively. Shading under points in (c) shows Mean Annual Precipitation (MAP). Arrows show maximum seasonal range in each variable – (a) Annual Range in Temperature (ART), (b) Annual Range in Salinity (ARS), and (c) Annual Range in Precipitation (ARP).

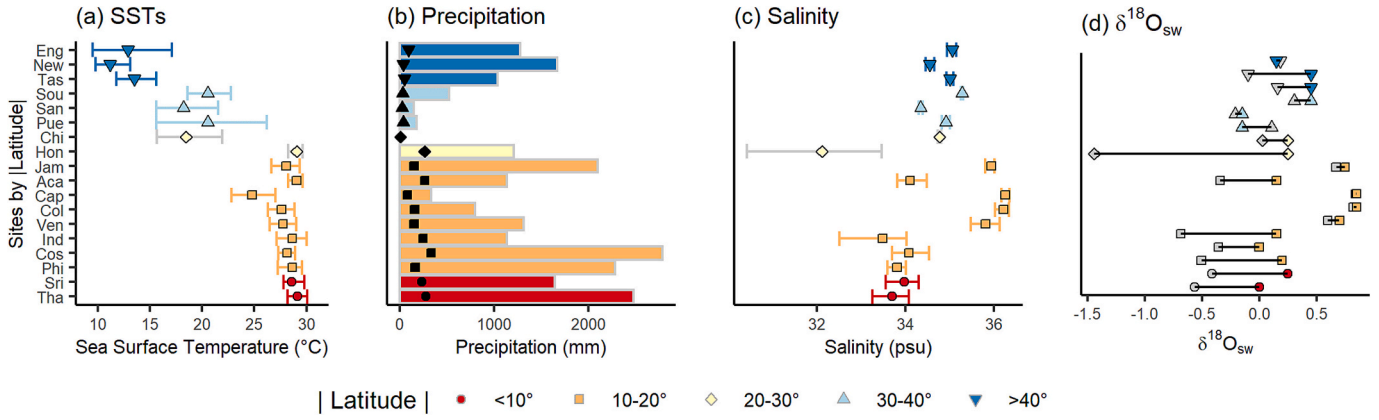

Fig. 3. Climatology for all sites, ordered by increasing latitude bottom to top, labeled with location codes as defined in Table 2. (a) SST, (b) precipitation, (c) salinity, and (d) $\delta^{18}O_{sw}$. In (a) and (c), points show annual means and bars show seasonal ranges. In (b), points show seasonal range (wettest minus driest month) and bars show total annual rainfall (MAP). In (d), colored points show $\delta^{18}O_{sw}$ value from the LeGrande and Schmidt (2006) interpolation, and linked gray points show $\delta^{18}O_{sw}$ values derived from mean annual salinity according to the equation in Brennan et al. (2012).

$$T = 20.6–4.34\left(\delta^{18}O_{carb} - \delta^{18}O_{sw} + 0.20\right)$$

Minimum and maximum $\delta^{18}O_{carb}$ values were compared to summer and winter monthly temperatures from a given location (see section 2.3). Given the sampling resolution and resolution of climate data, comparison at the monthly scale is warranted. The mean and midpoint $\delta^{18}O_{carb}$ values were compared to the MASST at the shell location. In addition to individual shell estimates, we also calculated locality averages by averaging minimum, maximum, and mean/midpoint $\delta^{18}O_{carb}$ values from all shells from each location and then converting to temperature using the site-specific $\delta^{18}O_{sw}$ value.

Using the instrumental range in SST determined for each site, we first calculate the SST equivalent in $\delta^{18}O_{carb}$. This value is the range in shell $\delta^{18}O_{carb}$ values that would expected from seasonal temperature change alone:

$$\delta^{18}O_{carb\ SST\ eq.} = 0.23^{*}\ (SST_{max}–SST_{min})$$

where the coefficient of 0.23 is the experimentally derived relationship between aragonite $\delta^{18}O_{carb}$ and temperature found in Grossman (2012) and SST_{max} and SST_{min} are the extremes of monthly mean values for a given site (see section 3.2). This SST equivalent in $\delta^{18}O_{carb}$ is then subtracted from the measured range in $\delta^{18}O_{carb}$ in each shell:

$$\text{apparent range in } \delta^{18}O_{sw} = \left(\delta^{18}O_{carb,max}–\delta^{18}O_{carb,min}\right)–0.23^{*}\ (SST_{max}–SST_{min})$$

2.5. Calculation of apparent range in $\delta^{18}O_{sw}$

One way to separate the competing effects of temperature and $\delta^{18}O_{sw}$ is to calculate the "apparent range in $\delta^{18}O_{sw}$" (Scholz et al., 2020). This method estimates the amount of influence that annual SST change alone should have on the range in $\delta^{18}O_{carb}$, subtracts that from the measured range and uses the residual as an estimate of $\delta^{18}O_{sw}$ variability.

This calculation estimates how much $\delta^{18}O_{carb}$ varies beyond the variation expected from temperature alone. This additional variation is assumed to be caused by seasonal changes in $\delta^{18}O_{sw}$. If the apparent range in $\delta^{18}O_{sw}$ is positive, this indicates that variations in $\delta^{18}O_{sw}$ are amplifying the $\delta^{18}O_{carb}$ range. If the apparent range in $\delta^{18}O_{sw}$ is negative, this indicates that variations in $\delta^{18}O_{sw}$ are dampening the $\delta^{18}O_{carb}$ range. The apparent range in $\delta^{18}O_{sw}$ is only quantitatively accurate if

$\delta^{18}O_{sw}$ is varying exactly in-phase with temperature (alignment of $\delta^{18}O_{sw}$ and temperature extrema). Nevertheless, the apparent range in $\delta^{18}O_{sw}$ is a useful way to estimate the magnitude and direction of influence of possible $\delta^{18}O_{sw}$ changes.

3. Results

3.1. Seasonal climate and seawater data

Temperature, precipitation, and salinity regimes varied widely across the 18 sites (Fig. 3). Mean annual sea surface temperature (MASST) varied from a low of 12.6 °C in England to a high of 28.9 °C in Acapulco, Mexico. The annual range in SST (ART) was lowest in tropical locations, with the smallest annual range (1.6 °C) in Costa Rica. Mid-latitude sites had higher annual temperature ranges (e.g. England, ART = 7.6 °C), as expected given their latitude. The highest ART (10.4 °C) was recorded in Puerto Penasco, Mexico, despite its subtropical latitude (Fig. 3a), likely due to the Gulf of California's unique seasonal gyre (Lavín et al., 2014). Preindustrial SSTs (1890–1910) were 0.6 °C cooler on average, but spatial patterns were unchanged (Fig. S3).

Both mean annual precipitation (MAP) and the annual range in precipitation (ARP) were lowest in Chile, which experienced a total rainfall of only 7 mm and only 3 mm difference between the wettest and driest months. Other sites with low ARP were San Felipe and Puerto Penasco, Mexico, and New Zealand (all <40 mm variation seasonally). MAP and ARP were highest in Costa Rica, with a MAP of 2788 mm and a variation of 331 mm between the wettest and driest months. Other tropical sites such as Jamaica, Thailand, and the Philippines also had high MAPs of greater than 2000 mm (Fig. 3b).

In most studied sites, the rainiest season was positively correlated with the warmest season with a phase lag ≤2 months ($n = 11/18$ sites) (Table 2, Fig. S2). Other sites showed a positive correlation between precipitation and temperature with a larger phase lag ($n = 3/18$), a negative correlation with ≤2 months phase lag ($n = 2/18$) or a negative correlation with a 3+ month phase lag (n = 2/18). Correlations were strong, with $R > |0.7|$ in 12 of 18 sites.

Mean annual salinity (MAS) varied from 32.1 psu in Hong Kong, to 36.3 psu in Cape Verde. MAS was highest around ~20 degrees latitude and was lower in both the tropics and higher latitudes (Fig. 3c). This follows global patterns of increased salinity in the subtropics due to increased evaporation, and decreased salinity near the equator due to high amounts of precipitation. The annual range in salinity (ARS) was lowest in South Africa (0.1 psu), and highest in Hong Kong (3.1 psu). This high salinity variation in Hong Kong is due to the competing influences of saline waters from the South China Sea and freshwater from the Pearl River (Morton and Morton, 1983). This river delivers 336 km^3 of freshwater outflow annually, 80 % of which occurs during the flood season from April to September (Zhang et al., 2007). *Turritella bacillum* is known to occur in waters strongly influenced by this discharge (Shin et al., 2020).

The annual range in salinity (ARS) is strongly correlated with the annual range in precipitation (ARP) at all sites (Fig. 4a), with the notable exception of two outliers: India and Hong Kong. This may be due to the delivery of fresh water by large rivers with broader watersheds, the Kaveri/Uppanar River in the case of Tharangambadi, India, and the Pearl River in the case of Hong Kong. These sites were excluded from the linear regression shown in Fig. 4a.

$\delta^{18}O_{sw}$ values from the LeGrande and Schmidt (2006) interpolation varied from −0.15 ‰ in Puerto Penasco, Mexico to +0.85 ‰ in Cape Verde. These interpolated values are higher than those calculated from the empirical equation in Brennan et al. (2012), which is based on mean annual salinity (Fig. 3d). The discrepancy is particularly large for sites with high seasonal ranges in salinity, such as Hong Kong. The relationship from Brennan et al. (2012) is based on data limited to salinities >34 psu, and can lead to spurious $\delta^{18}O_{sw}$ values in lower salinity environments. This may explain the larger discrepancies between the methods of estimation in tropical sites, and in Hong Kong in particular. In this study we opt to use the LeGrande and Schmidt (2006) values, as they include more spatial variability in the $\delta^{18}O_{sw}$-salinity relationship and better represent lower salinity environments.

$\delta^{18}O_{sw}$ values from the LeGrande and Schmidt (2006) interpolation are highest in the extratropics and lower in both the tropics and higher latitudes, following salinity patterns. Across all study sites, mean annual salinity was correlated with $\delta^{18}O_{sw}$ values from LeGrande and Schmidt (2006) (Fig. 4b), with an approximate slope of 0.32 and an intercept of 10.6, similar to the relationship found in Brennan et al. (2012) despite significantly fewer points ($\delta^{18}O_{sw}$ values estimated using the equation from Brennan et al. (2012) are, by definition, correlated to local salinity).

Temperature and salinity were also correlated in time in all sites. Warmer seasons correlated with locally lower salinity in 11 of 18 sites (Table 2). Correlations were high, with 16 out of 18 locations having maximum correlation coefficients $R > |0.7|$. Lower salinity correlating with the warmest season would amplify seasonality in $\delta^{18}O_{carb}$. Although seasonal-scale $\delta^{18}O_{sw}$ data do not exist, based on the correlation between mean annual salinity and $\delta^{18}O_{sw}$, it could be inferred that a similarly high percentage of sites may show a negative, in-phase correlation between seasonal temperature and $\delta^{18}O_{sw}$, in which the lowest $\delta^{18}O_{sw}$ values coincides with the warmest season.

Table 2
Cross correlation function between monthly temperatures/precipitation and temperatures/salinities at each location, from reanalysis data. Maximum correlation coefficient values (R) are colored from −1 (red) to +1 (blue), Lag values of maximum correlation (in months) is bolded when ≤2 months in either direction.

		Temperature/ Precipitation		Temperature/ Salinity	
Location	Code	Max R	Lag (mos)	Max R	Lag (mos)
Cape Verde	Cap	+0.81	**1**	+0.91	**1**
Antofagasta, Chile	Chi	+0.65	**0**	+0.93	**0**
Guajira Peninsula, Columbia	Col	+0.83	**0**	−0.93	**0**
Playa Avellana, Costa Rica	Cos	+0.77	**−1**	−0.74	−3
Plymouth Harbor, England	Eng	+0.84	−3	+0.85	−3
Hong Kong	Hon	+0.80	**0**	−0.81	**0**
Tharamgambadi, India	Ind	+0.59	−5	+0.81	**0**
Jamaica	Jam	+0.76	**0**	−0.76	**−2**
Stewart Island, New Zealand	New	+0.39	**−2**	−0.94	**−1**
Acapulco, Mexico	Aca	+0.80	**0**	−0.94	**−2**
Puerto Penasco, Mexico	Pue	+0.59	**0**	−0.97	**0**
San Felipe, Mexico	San	−0.62	**2**	−0.65	**1**
Cebu City, Philippines	Phi	+0.87	**−1**	−0.87	−3
Jeffreys Bay, South Africa	Sou	−0.66	−4	−0.87	**0**
Sri Lanka	Sri	+0.73	−6	+0.57	−4
Cape Grim, Tasmania	Tas	−0.91	**1**	+0.91	**−2**
Phang Nga Bay, Thailand	Tha	−0.71	3	+0.71	**1**
Carupano, Venezuela	Ven	+0.72	**1**	−0.91	**−1**

3.2. Turritellid isotopic data

$\delta^{18}O$ values for newly measured samples ranged from −3.32 to +2.37 ‰. Within a single shell, the $\delta^{18}O$ range (minimum to maximum $\delta^{18}O$ value) varied from 0.77 to 2.81 ‰ (Fig. 5, Table S1). Mean $\delta^{18}O$ values varied from −2.55 to +1.80 ‰, and were generally correlated with latitude, with higher latitude sites having higher average $\delta^{18}O$ values and vice versa. Midpoints varied from −2.47 to +1.83 ‰, and were |0.14 ‰| away from mean values, on average.

Most $\delta^{18}O$ profiles were sinusoidal in nature, showing smoothly alternating peaks and troughs, indicating the full seasonal range in conditions was likely captured in these records. However, some specimens showed signs of potential seasonal aliasing: one sample from India

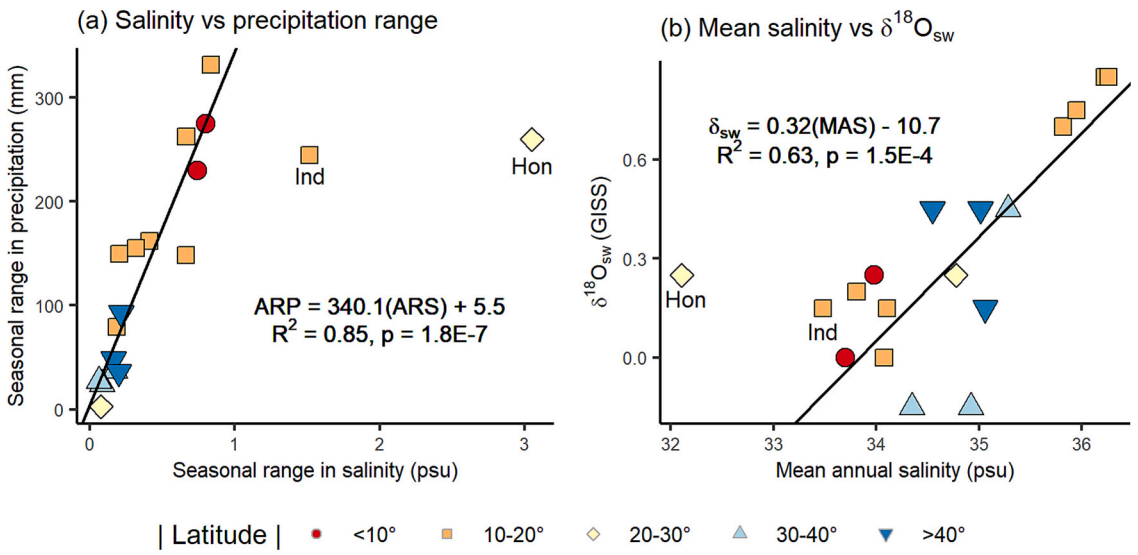

Fig. 4. (a) Annual range in precipitation (ARP) vs annual range in salinity (ARS), and regression line. (b) $\delta^{18}O_{sw}$ from LeGrande and Schmidt, 2006, vs mean annual salinity, with regression line. Regression does not include two outlier locations with exceptionally high seasonal salinity ranges [India (orange) and Hong Kong (yellow)]. (For interpretation of the references to color in this figure legend, the reader is referred to the web version of this article.)

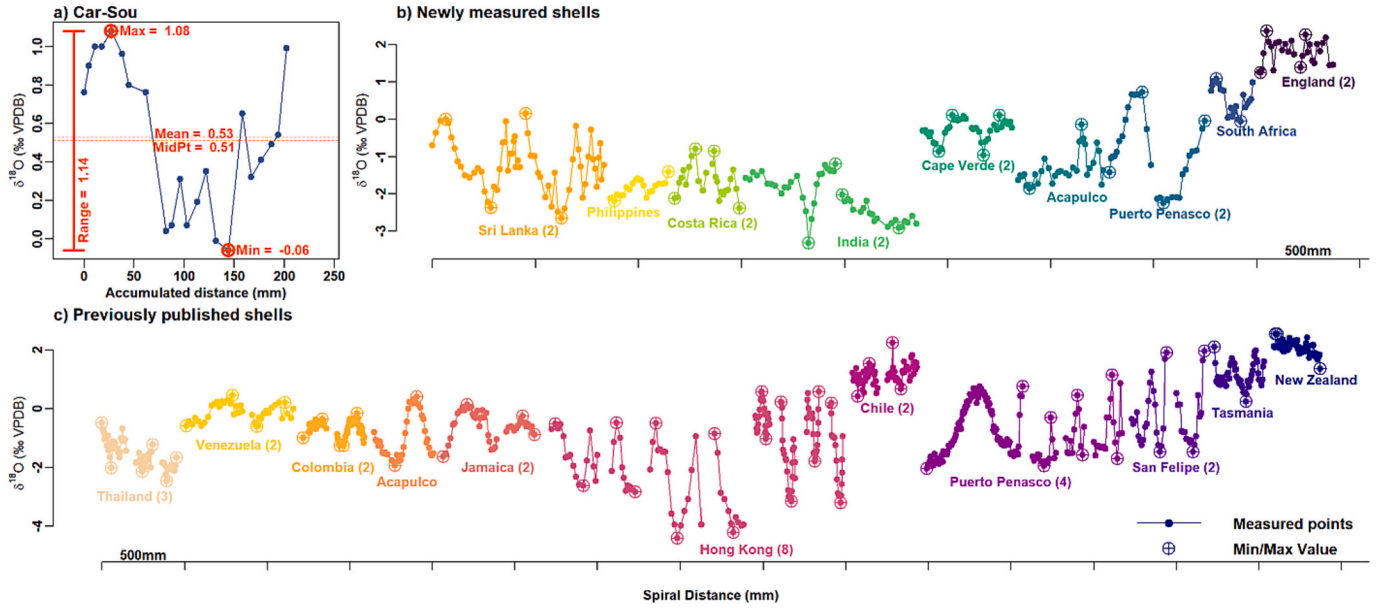

Fig. 5. $\delta^{18}O$ profiles of all newly measured (b) and previously published (c) turritellid shells, arranged by increasing absolute value of site latitude. Distance along each specimen is measured in the spiral growth direction, Statistics for all profiles were calculated as shown in (a), including minimum, maximum, mean, midpoint, and total range. Profiles are labeled by location, with the number of specimens in parentheses.

showed sharper, sometimes single-point peaks/troughs, which could indicate growth slowdown or stoppage during certain seasons or rapid changes in $\delta^{18}O_{sw}$. To test the effects of single point extrema, we recalculated $\delta^{18}O_{carb}$ ranges after removing the minimum and maximum $\delta^{18}O_{carb}$ value of each shell. These adjusted ranges were not significantly different, indicating that sampling resolution was sufficient to fully capture the range present in each shell. The majority of shells recorded at least 1 year of growth, with estimated lifespans of 1–3 years, consistent with observations from other turritellids (e.g. Anderson and Allmon, 2020). Only 5 out of 43 shells showing monotonic $\delta^{18}O$ profiles that indicate less than a full year of growth and the potential for an underestimation of seasonal ranges.

$\delta^{13}C_{carb}$ values for newly measured samples ranged from +0.12 ‰ to +3.83 ‰, with individual intrashell ranges varying from 0.54 ‰ to 2.17 ‰ (Fig. S4). $\delta^{13}C$ profiles showed less coherent subannual/seasonal variations, though most samples did tend to decrease in $\delta^{13}C_{carb}$ throughout their lifetime. Although some shells showed significant correlation between $\delta^{18}O_{carb}$ and $\delta^{13}C_{carb}$, across the population as a whole, correlations varied, with no systematic pattern found (Fig. S5).

3.3. Reconstructed mean annual temperatures

For each shell profile, estimates of MASST were calculated both from the shell mean and midpoint $\delta^{18}O$ values, using the calibration from Grossman (2012) and assuming a fixed $\delta^{18}O_{sw}$ value from LeGrande and Schmidt (2006) (Fig. 6a, b). When compared to instrumental MASST values, both means and midpoints provide reasonable estimates, as indicated by low root mean square error (RMSE) values, estimating the

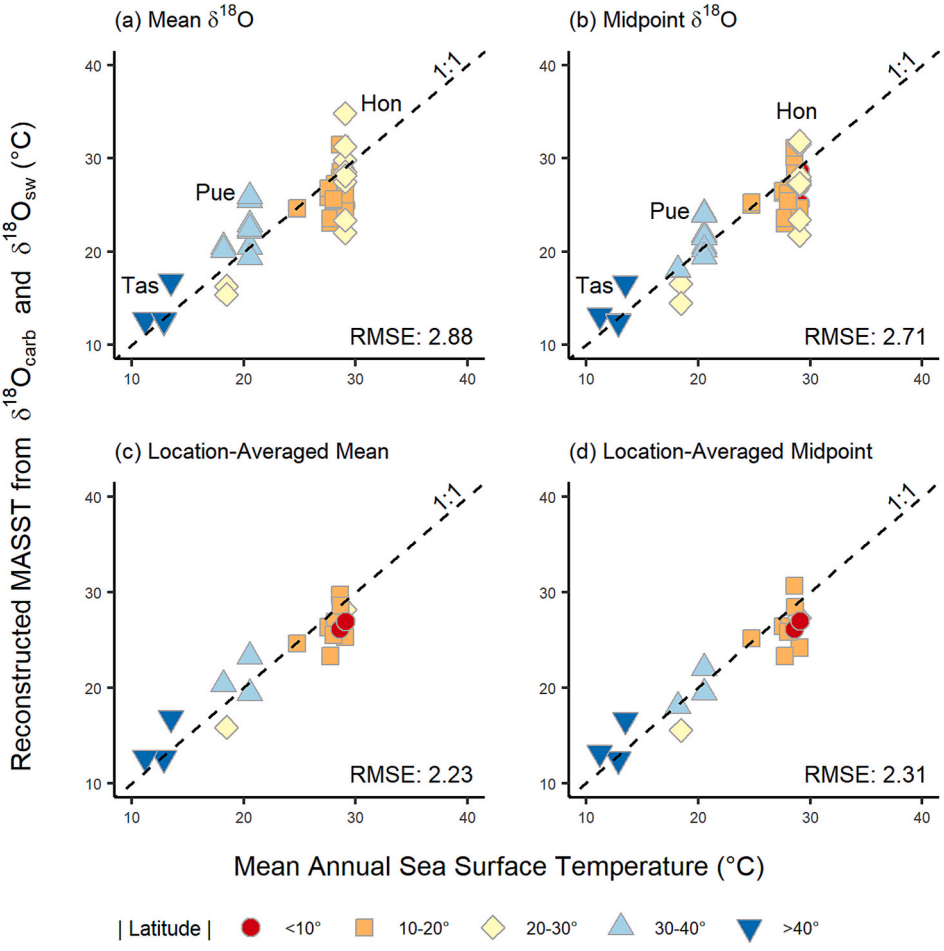

Fig. 6. Reconstructed MASST compared to observed MASST. Reconstructed MASST was calculated using the measured $\delta^{18}O_{carb}$ mean (a), and midpoint (b), assuming a locality-specific $\delta^{18}O_{sw}$ values from LeGrande and Schmidt (2006). Location averages were calculated by combining all $\delta^{18}O$ data from shells from that location then determining the mean (c) and midpoint (d) values and using that to estimate MASST along with the same locality-specific $\delta^{18}O_{sw}$ value. Color corresponds to the absolute value of latitude and the dashed line represents a 1:1 line comparing observed to reconstructed MASST values. Outliers are labeled by location codes.

amount of divergence from a 1:1 line. The RMSE values of individual shell mean and midpoint values are 2.88 and 2.71, respectively. Means or midpoints from all shells at each location were combined to compute the location-averaged midpoint and mean estimate of MASST (6c, d). The RMSE for the location-averaged mean and midpoint were very similar (2.23 compared to 2.31), and both were lower than single-shell statistics, emphasizing the benefits of sampling more than one shell per location. An ordinary least squares regression for the location-averaged means yields the following relationship:

$$\text{Reconstructed MASST} = (0.80 \pm 0.07)\text{*Instrumental MASST} + (4.0 \pm 1.7)$$

$$R^2 = 0.88, p < 4E-9$$

The linear fit for midpoints has nearly identical coefficients. Both regressions indicate a positive bias of 4 °C at 0 °C, no bias at 20 °C, and a slight cold bias at temperatures >20 °C.

3.4. Reconstructed seasonal temperatures

Winter and summer seasonal temperature estimates were calculated using the minimum (summer) or maximum (winter) $\delta^{18}O_{carb}$ value for each shell, again assuming a fixed, locality-specific $\delta^{18}O_{sw}$ taken from LeGrande and Schmidt (2006). Reconstructed summertime temperatures were frequently higher than instrumental temperatures in both single-shell and location-averaged approaches (Fig. 7a, c), with some samples from Hong Kong showing expected temperatures of near 40 °C (Fig. 7a, yellow diamonds). The average offset for all samples is +0.87 °C. Averaging by location reduces the total RMSE from 3.33 to 2.55 and reduces the average offset to +0.55 °C. Samples from Hong Kong and India had particularly high reconstructed summertime temperatures, which may indicate that the assumed annual average $\delta^{18}O_{sw}$ value is likely higher than actual summertime $\delta^{18}O_{sw}$ in these regions.

Reconstructed wintertime temperatures are colder than observed values, with a mean offset of −3.07 °C. Averaging by location reduces the RMSE from 4.77 to 3.97 and the mean offset to −2.59 °C, but does not remove the cold-bias. Specimens from Hong Kong, Sri Lanka, and Acapulco showed particularly cold temperature estimates. If instead $\delta^{18}O_{sw}$ values are estimated from MAS according to the equation from Brennan et al. (2012) (Fig. 3d), calculated temperatures are lower by ~2–3 °C across the board, reducing both reconstructed summer and winter temperatures while not affecting seasonal ranges.

With a warm bias to summertime temperatures and a cold bias to wintertime temperatures, $\delta^{18}O$-based reconstructions of the annual range in temperatures (ART) assuming invariant $\delta^{18}O_{sw}$ almost universally overestimate the instrumental ART (Fig. 7c, f). The average overestimation is +3.9 °C, with the seasonal range calculated from individual shells ranging from 3.7 °C below to 15.5 °C above instrumental ART. Shells from locations such as Hong Kong and Sri Lanka had particularly egregious overestimations of ART, more than 10 °C above the instrumental value. In contrast, shells from Chile and Puerto

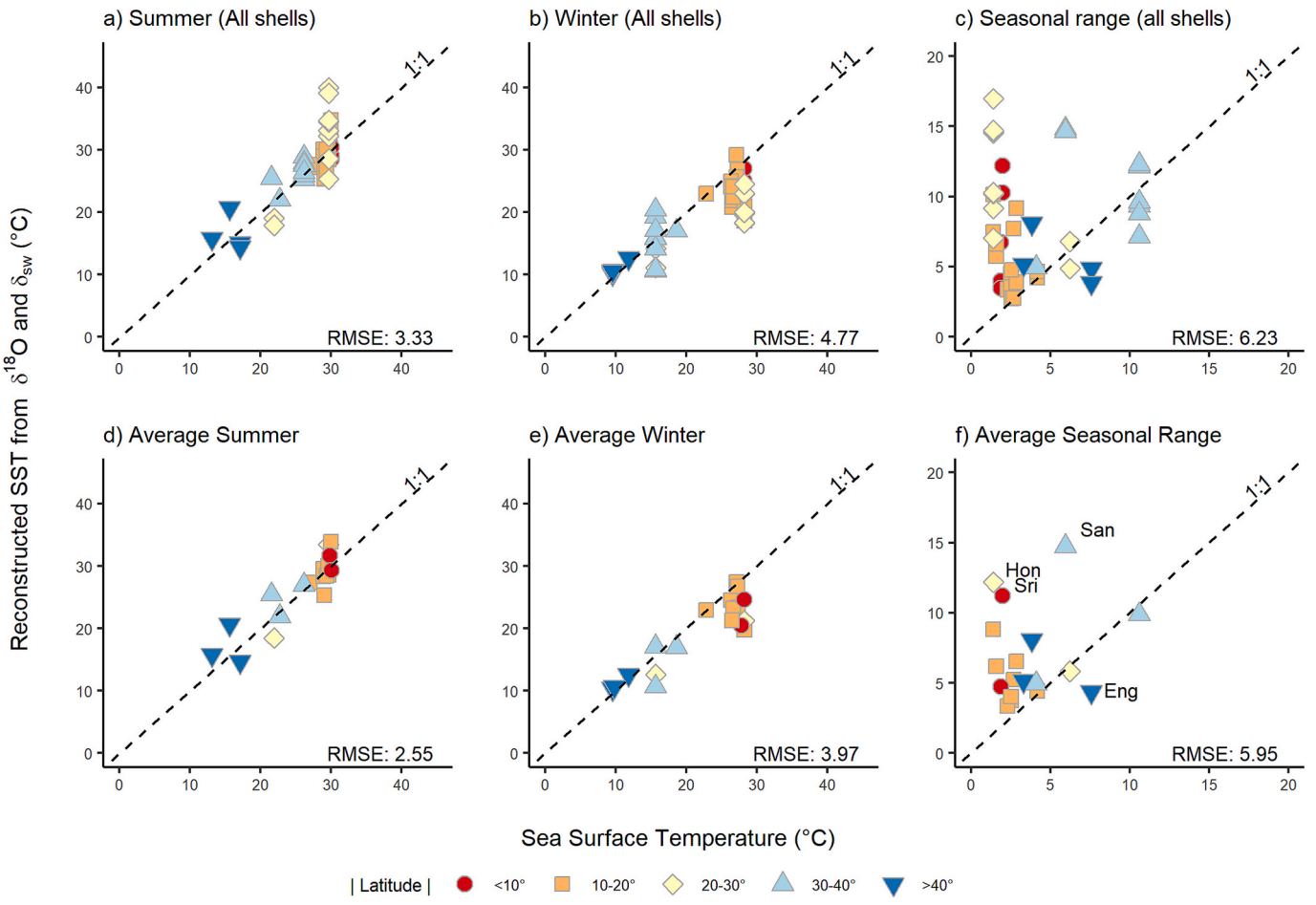

Fig. 7. Reconstructed seasonal SST in the summer (a) and winter (b) for all shells. Location-averaged expected SST values in the summer (d) and winter (e). Expected seasonal range in SST calculated from shells assuming constant δ^{18}Osw vs. the observed seasonal SST range at each location, for (c) all shells and (f) averages of shells by location. Outliers are labeled by location codes. Color coding as in previous figs.

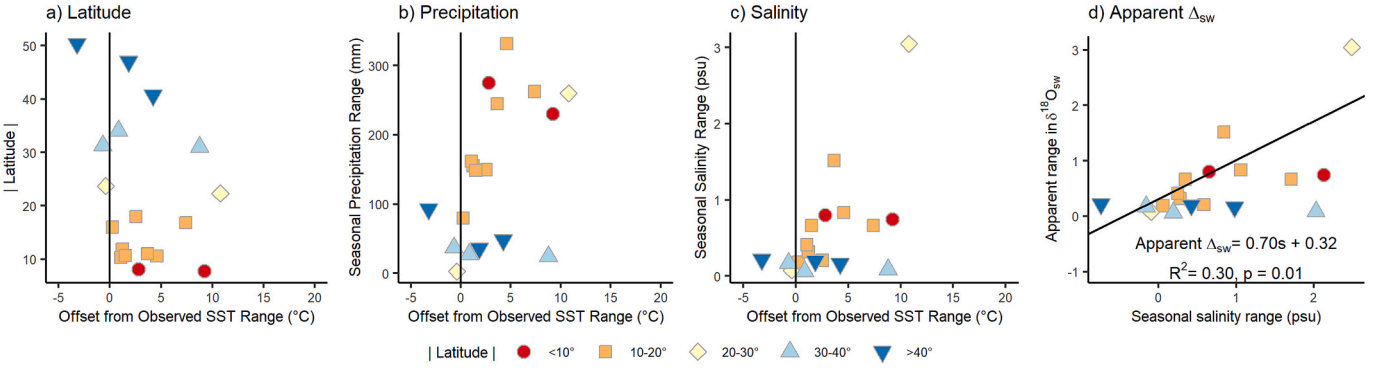

Fig. 8. Offset (difference) between the expected seasonal SST range from $\delta^{18}O_{carb}$ assuming a fixed $\delta^{18}O_{sw}$ and the observed seasonal range in SST (x-axis) for the location-average of all shells, and its association with (a) latitude, (b) seasonal range in precipitation, and (c) seasonal range in salinity. (d) Location averages of apparent range in $\delta^{18}O_{sw}$, calculated as the observed range in $\delta^{18}O_{carb}$ minus the approximate contribution from seasonal temperature range, vs. the seasonal salinity range at each site. Linear regression shows a significant positive relationship with $R^2 = 0.30$. $p = 0.01$.

Penasco, Mexico predicted the instrumental ART to within ~0.1 °C. The primary exception to the trend of overestimation was the site in England, which underestimated seasonality by 3.2 °C.

This separation between sites with large overestimations and little to no overestimations aligns with local variability in precipitation and salinity (Fig. 8). Locations with high ARP and ARS (e.g. Hong Kong) showed larger overestimations of ART, whereas arid regimes with low seasonality of precipitation and salinity (Puerto Penasco and Chile) more accurately estimate ART.

The apparent range in $\delta^{18}O_{sw}$ is another way to quantify the disagreement between the actual $\delta^{18}O_{carb}$ range and that expected from instrumental SST variability. Most sites suggest variability of <1 ‰ in $\delta^{18}O_{sw}$. There is a correlation between the seasonal salinity range and the apparent range in $\delta^{18}O_{sw}$ (Fig. 8), reflecting the connection between processes influencing salinity and $\delta^{18}O_{sw}$ locally. In particular, Hong Kong has both a very high annual range in salinity and apparent range in

$\delta^{18}O_{sw}$, which may reflect seasonal circulation shifts that bring more or less freshwater to the coastal areas via the Pearl River (Zhang et al., 2007). Sites with the lowest ARS such as Chile and Puerto Penasco, Mexico, show apparent ranges in $\delta^{18}O_{sw}$ of closer to zero. Significant outliers to this relationship include the sites San Felipe and Acapulco (Mexico), and Sri Lanka.

4. Discussion

4.1. Turritellids as recorders of MASST

Turritellids are fast growing and globally abundant since the Cretaceous, making them a potential paleoclimatic archive for a wide range of geographic locations and time periods. To date, more than 40 fossil species and around 100 fossil turritellid specimens have been sampled isotopically in paleoclimatic contexts (e.g. Jones and Allmon, 1995; Andreasson and Schmitz, 1996, 1998, 2000). To validate paleoclimatic reconstructions from these species, it is crucial to better understand how well turritellids record annual mean and subannual climate in a modern context.

We find that turritellid shells analyzed in this and previous studies accurately record MASST, albeit with some slight, non-systematic biases. The linear regression of temperatures estimated from $\delta^{18}O_{carb}$ and $\delta^{18}O_{sw}$ indicates a slight warm bias at SSTs <20 °C, and a slight cold bias at SSTs >20 °C. Using the mean or midpoint of the $\delta^{18}O$ profiles yields similar results, indicating that turritellids may not have substantial seasonal growth biases or growth shutoffs in the studied habitats. Seasonal growth biases would be expected to reduce summer extremes and/or increase winter minima, leading to an underestimation in seasonal range and a misrepresentation of MASST by both the mean and midpoint methods. Underestimation of seasonal range is only observed in one site (England, Fig. 7e). This may be due to growth stoppages, which have previously been observed in high-latitude specimens of *Maoricolpus roseus* (Scot, 1997), though the isotopic profiles do not appear to be seasonally truncated. However, all other sites showed overestimation of seasonal ranges. Accuracy of the reconstructed temperature improves by averaging multiple shells from the same location (Fig. 6), supporting the benefits of analyzing multiple shells from a single site in order to achieve a more accurate estimate of MASST.

The estimation of MASST is clearly complicated by imperfect knowledge of mean $\delta^{18}O_{sw}$. $\delta^{18}O_{sw}$ estimates from Brennan et al. (2012) and LeGrande and Schmidt (2006) differ greatly at some sites (Fig. 3), and the Brennan et al. (2012) relationship becomes increasingly uncertain at low salinities (<32 psu), which may lead to difficulties in some of the salinity-stressed coastal settings that turritellids inhabit. We use the interpolated $\delta^{18}O_{sw}$ values from LeGrande and Schmidt (2006) for our temperature estimations in this study, but this is also uncertain, with many regions having few nearby measurements of $\delta^{18}O_{sw}$ to rely on. However, knowledge of mean $\delta^{18}O_{sw}$ is key to getting an accurate estimate of MASST. This poses a significant challenge in paleoclimate contexts: to address this uncertainty, $\delta^{18}O_{carb}$ sclerochronology of turritellids should be paired with another method that can independently constrain $\delta^{18}O_{sw}$, such as the clumped isotope paleothermometer (Δ_{47}) or paired Mg/Ca and $\delta^{18}O_{carb}$ measurements.

Finally, the lack of systematic bias in $\delta^{18}O_{carb}$-based estimates of MASST may also suggest turritellids do not suffer from significant vital effects. Biologically-derived isotopic fractionations, or BioDIFs (Curley et al., 2023), are caused by disequilibrium precipitation and/or precipitation from a growth fluid that differs from surrounding seawater, biasing shell isotopic composition and typically presenting as a systematic, unidirectional bias in $\delta^{18}O_{carb}$ or reconstructed MASST. However, these two mechanisms of BioDIF (disequilibrium precipitation and fractionated growth fluid composition) could possibly cancel each other out in $\delta^{18}O_{carb}$, obscuring the typical indicator of the presence of a vital effect. Clumped isotope paleothermometry (Δ_{47}) can isolate the presence of disequilibrium precipitation, especially in conjunction with Δ_{48} (Fiebig et al., 2021; Curley et al., 2023), as deviations in clumped isotope temperature from environmental temperature are uniquely caused by disequilibrium precipitation and are independent of fluid composition. This method should be applied to turritellids in a future study to confirm our conclusions on the robustness of $\delta^{18}O_{carb}$-based MASST reconstructions in this archive.

4.2. Turritellids as recorders of seasonal temperature ranges

Previous calibrations of turritellids performed by Allmon et al. (1992) and Teusch et al. (2002) found that the $\delta^{18}O_{carb}$ provided accurate estimates of both mean SST and seasonal SST ranges. The common factor between both these studies is that the sites (Puerto Penasco, Mexico and Antofagasto, Chile) had very low seasonal variability in both salinity and precipitation, meaning that the seasonal changes in $\delta^{18}O_{sw}$ were far smaller than the effect of the seasonal temperature changes. Our study shows that in most other regions, this is not the case, and that neglecting seasonal variations in $\delta^{18}O_{sw}$ can lead to inaccurate estimates of seasonal temperature ranges (Fig. 8).

Climate data from all locations indicate that 11/18 sites have a positive correlation between temperature and precipitation (Table 1, Fig. S2), meaning peak freshwater delivery (and by inference, minimum $\delta^{18}O_{sw}$ and salinity values) should coincide with peak temperatures. Mean annual salinities also correlate well with mean $\delta^{18}O_{sw}$ values across sites (Fig. 4). Although we don't have seasonal-scale $\delta^{18}O_{sw}$ measurements, one can infer that seasonal changes in salinity would correspond to seasonal changes in $\delta^{18}O_{sw}$. Taken together, this suggests that a high percentage of our study sites would have the lowest $\delta^{18}O_{sw}$ coinciding with peak temperatures, and vice versa, amplifying the seasonal range in $\delta^{18}O_{carb}$ above that expected from temperature variations alone. Not taking into account these $\delta^{18}O_{sw}$ variations and assuming an annual fixed $\delta^{18}O_{sw}$ value would therefore result in an overestimation of ART.

Our data show that typical methods of converting $\delta^{18}O_{carb}$ profiles of turritellids to seasonal temperature profiles do indeed overestimate of the annual range in temperature (ART) in many sites (Fig. 7). This occurs through both an overestimation of both summertime maxima and wintertime minima. There is an association between sites with higher seasonal variations in precipitation and salinity and sites that overestimate ART (Fig. 8). We suggest this is due to seasonally variable delivery of rainwater to the coastal areas, either through direct rainfall on the ocean surface, riverine delivery of continental runoff, or submarine groundwater discharge. This freshwater would be isotopically depleted relative to seawater, resulting in seasonal variations in coastal $\delta^{18}O_{sw}$. This is most clearly seen in the samples from Hong Kong, and Sri Lanka, which overestimated the seasonal range in SST by over 10 °C (Fig. 7f) and show strong positive correlations between seasonal temperature and precipitation (Table 2). In contrast, the samples from locations with low seasonality of precipitation and salinity, like Puerto Penasco and Chile, accurately record the observed SST range (Fig. 7e), as found in previous studies.

In paleoclimate applications, Jones and Allmon (1995) and Andreasson and Schmitz (1996, 1998, 2000) used turritellid $\delta^{18}O_{carb}$ profiles to reconstruct annual SST ranges during the Pliocene and early-middle Eocene, respectively, by assuming $\delta^{18}O_{sw}$ was constant throughout the year. We suggest that without prior knowledge of the paleoenvironment and seasonal changes in $\delta^{18}O_{sw}$, these estimates SST ranges are likely to be overestimates. In contrast, when Miocene turritellids from equatorial Colombia showed a much higher range in $\delta^{18}O_{carb}$ than expected for the minimally-seasonal tropics, Scholz et al. (2020) assumed that the temperature seasonality was minor and inferred that large observed range in shell $\delta^{18}O_{carb}$ instead represented significant changes in coastal salinity. These salinity changes were hypothesized to be driven by increased seasonality of precipitation and freshwater delivery in the Miocene relative to today, a conclusion supported by additional paleontological evidence for a wet, brackish

paleoenvironment. In this case, the extreme low latitude of the site supported the assumption of minimal temperature seasonality and stronger impact of seasonal precipitation.

Given the apparent influence of seasonal $\delta^{18}O_{sw}$ on turritellid profiles, we suggest using caution when interpreting their profiles to constrain subannual paleoenvironmental variations. Consideration of the fossil assemblage may help ascertain if the specimens inhabited more salinity-stressed regions, or were fully marine: the presence of stenohaline taxa and little evidence of wave reworking may suggest that the specimens were less affected by nearshore processes. However, in the absence of additional evidence suggesting fully-marine conditions, we suggest that turritellids are unlikely to faithfully record subannual temperature ranges due to the influence of seasonal $\delta^{18}O_{sw}$ changes. On the other hand, other mollusks that live in deeper shelf settings can be biased in the other direction, recording reduced seasonality due to temperature stratification with depth (e.g. Johnson et al., 2021), so should also be treated with caution. Perhaps the best approach would therefore be to analyze a range of species and interpret their resulting profiles in context of their preferred depth habitats.

4.3. Gleaning information on paleohydrology from $\delta^{18}O_{carb}$ profiles

Although the above finding that $\delta^{18}O_{carb}$ profiles tend to overestimate ART in nearshore, shallow-water-dwelling turritellids could be seen as disappointing, it can also be a new source of information on paleohydrology. Specifically in tropical sites, where the assumption of a low seasonality in temperature is more robust, variations in the amplitude of $\delta^{18}O_{carb}$ profiles can instead be inferred to reflect changes in the seasonal variability in salinity or precipitation (e.g. Scholz et al., 2020). The apparent range in $\delta^{18}O_{sw}$ calculation is one way to estimate the extent of the impact of local variations in salinity and precipitation (Fig. 8d), though it is limited by the assumption that temperature and salinity/precipitation vary in phase. Offsets from assumed SST range are another way to estimate the potential influence of $\delta^{18}O_{sw}$ changes (Fig. 8c). Although not a quantitative proxy for past seasonal rainfall or salinity changes, these alternate methods of interpreting $\delta^{18}O_{carb}$ profiles can be combined with other qualitative proxies like floral and faunal changes to indicate changes to a location's rainfall regime over time.

This finding is not restricted to turritellid gastropods. Although subannual variations in $\delta^{18}O_{sw}$ are often ignored in sclerochronological studies analyzing deep-dwelling species, any marine calcifiers living in shallow, coastal environments should similarly be affected by variable $\delta^{18}O_{sw}$, and may therefore be subject to the similar complexities in the interpretation of their sclerochronological records.

5. Conclusions

Turritellids are an under-studied yet extremely widespread family with a variety of potential paleoclimate applications. Their shallow, nearshore habitat means that they are subject to the influence of many more factors that deep-water organisms. The complexity and ambiguity of these records can be frustrating in some ways, as it makes disentangling the multiple signals and variables difficult. However, it also means that this sclerochronological data are rich with multiple types of information about the climate, if we can figure out how to properly extract it.

Our combined dataset of 43 $\delta^{18}O_{carb}$ profiles suggests turritellids accurately record MASST, given accurate local $\delta^{18}O_{sw}$ values. However, in most of our study sites, local precipitation, salinity and $\delta^{18}O_{sw}$ changes amplify the subannual $\delta^{18}O_{carb}$ signal recorded in turritellids. This leads to an overestimation of the annual range in temperature. Although this is unfortunate from a paleo-temperature proxy perspective, it may provide a new way of qualitatively assessing seasonal paleohydrology, especially in tropical sites with low temperature seasonality.

This study highlights the need for clear knowledge of $\delta^{18}O_{sw}$, both mean values and seasonal variability, in order to accurately reconstruct temperatures from $\delta^{18}O_{carb}$. More modern $\delta^{18}O_{sw}$ measurements are need to better document spatial and temporal variability in the modern ocean. In paleoclimate studies, use of independent methods to constrain $\delta^{18}O_{sw}$ should be applied whenever possible to anchor paleotemperature estimates based on $\delta^{18}O_{carb}$. Estimates of local salinity or $\delta^{18}O_{sw}$ and its seasonal variations are key to accurately reconstruct SST from turritellid sclerochronologies.

CRediT authorship contribution statement

Serena R. Scholz: Writing – review & editing, Writing – original draft, Visualization, Methodology, Investigation, Formal analysis, Data curation, Conceptualization. **Sierra V. Petersen:** Writing – review & editing, Validation, Supervision, Resources, Methodology, Investigation, Conceptualization. **Brendan M. Anderson:** Writing – review & editing, Investigation.

Declaration of competing interest

The authors declare that they have no known competing financial interests or personal relationships that could have appeared to influence the work reported in this paper.

Data availability

All isotopic data are available in a supplemental csv file. All reanalysis datasets are freely available for download. ERSST v.5 is available from NOAA at https://www.ncei.noaa.gov/products/extended-reconstructed-sst. SODA 3.3.1 is available at https://www2.atmos.umd.edu/~ocean/. CRU 3.25 are available at https://crudata.uea.ac.uk/cru/data/hrg/cru_ts_3.25/.

Acknowledgements

The authors would like to thank L. Wingate and K. Lohman for technical support, and J. Cole and the University of Michigan Museum of Zoology for specimens. Scholz was partially supported by a Turner Research Grant. Petersen was supported by the Sloan Research Fellowship and NSF-EAR CAREER grant #2237429. Anderson is supported by NSF DEB 2225014.

Appendix A. Supplementary data

Supplementary data to this article can be found online at https://doi.org/10.1016/j.palaeo.2024.112553.

References

Allmon, W.D., 1988. Ecology of recent turritelline gastropods (Prosobranchia, Turritellidae): current knowledge and paleontological implications. Palaios 259–284.

Allmon, W.D., 2007. Cretaceous marine nutrients, greenhouse carbonates, and the abundance of turritelline gastropods. J. Geol. 115, 509–524.

Allmon, W.D., 2011. Natural history of Turritelline Gastropods (Cerithiodea: Turritellidae): a Status Report. Malacologia 54, 159–202. https://doi.org/10.4002/040.054.0107.

Allmon, W.D., Jones, D.S., Vaughn, N., 1992. Observations on the biology of Turritella gonostoma Valenciennes (Prosobranchia: Turritellidae) from the Gulf of California: the. Veliger 35, 52–63.

Allmon, W.D., Jones, D.S., Aiello, R.L., Gowlett-Homes, K., Probert, P.K., 1994. Observations on the biology of Maoricolpus roseus (Quoy and Gaimard) (Prosobranchia: Turritellidae) from New Zealand and Tasmania. Veliger 37, 267–279.

Anderson, B.M., Allmon, W.D., 2020. High calcification rates and inferred metabolic trade-offs in the largest turritellid gastropod, Turritella abrupta (Neogene). Palaeogeogr. Palaeoclimatol. Palaeoecol. 544, 109623. https://doi.org/10.1016/j.palaeo.2020.109623.

Anderson, B.M., Hendy, A., Johnson, E.H., Allmon, W.D., 2017. Paleoecology and paleoenvironmental implications of turritelline gastropod-dominated assemblages

from the Gatun Formation (Upper Miocene) of Panama. Palaeogeogr. Palaeoclimatol. Palaeoecol. 470, 132–146.
Andreasson, F.P., Schmitz, B., 1996. Winter and summer temperatures of the early middle Eocene of France from Turritella δ18O profiles. Geology 24, 1067–1070.
Andreasson, F.P., Schmitz, B., 1998. Tropical Atlantic seasonal dynamics in the early Middle Eocene from stable oxygen and carbon isotope profiles of mollusk shells. Paleoceanography 13, 183–192. https://doi.org/10.1029/98PA00120.
Andreasson, F.P., Schmitz, B., 2000. Temperature seasonality in the early middle Eocene from δ18O profiles of marine gastropod shells. GFF 122, 9–10. https://doi.org/10.1080/11035890001221009.
Avens, A.C., Sleigh, M.A., 1965. Osmotic balance in gastropod mollusks – I. Some marine and littoral gastropods. Comp. Biochem. Physiol. 16, 121–141.
Blay, J., Dongdem, F., 1996. Preliminary observations on the benthic macrofauna of a polluted coastal lagoon in Ghana (West Africa). Trop. Ecol. 37, 127–133.
Brennan, C.E., Weaver, A.J., Eby, M., Meissner, K.J., 2012. Modelling Oxygen Isotopes in the University of Victoria Earth System climate Model for Pre-industrial and last Glacial Maximum Conditions. Atmosphere-Ocean 50 (4), 447–465. https://doi.org/10.1080/07055900.2012.707611.
Buick, D.P., Ivany, L.C., 2004. 100 years in the dark: Extreme longevity of Eocene bivalves from Antarctica. Geology 32, 921. https://doi.org/10.1130/G20796.1.
Carton, J.A., Chepurin, G.A., Chen, L., 2018. SODA3: a new ocean climate reanalysis. J. Clim. 31, 6967–6983. https://doi.org/10.1175/JCLI-D-18-0149.1.
Crippa, G., Angiolini, L., Bottini, C., Erba, E., Felletti, F., Frigerio, C., Hennissen, J.A.I., Leng, M.J., Petrizzo, M.R., Raffi, I., Raineri, G., Stephenson, M.H., 2016. Seasonality fluctuations recorded in fossil bivalves during the early Pleistocene: Implications for climate change. Palaeogeogr. Palaeoclimatol. Palaeoecol. 446, 234–251. https://doi.org/10.1016/j.palaeo.2016.01.029.
Curley, A.N., Petersen, S.V., Edie, S.M., Guo, W., 2023. Biologically driven isotopic fractionations in bivalves: from palaeoenvironmental problem to palaeophysiological proxy. Biol. Rev. 98, 1016–1032. https://doi.org/10.1111/brv.12940.
De Winter, N.J., Vellekoop, J., Clark, A.J., Stassen, P., Speijer, R.P., Claeys, P., 2020. The giant marine gastropod Campanile giganteum (Lamarck, 1804) as a high-resolution archive of seasonality in the Eocene greenhouse world. Geochem. Geophys. Geosyst. 21 (4), e2019GC008794.
Dettman, D.L., Flessa, K.W., Roopnarine, P.D., Schöne, B.R., Goodwin, D.H., 2004. The use of oxygen isotope variation in shells of estuarine mollusks as a quantitative record of seasonal and annual Colorado river discharge. Geochim. Cosmochim. Acta 68, 1253–1263. https://doi.org/10.1016/j.gca.2003.09.008.
Fiebig, J., Daëron, M., Bernecker, M., Guo, W., Schneider, G., Boch, R., Bernasconi, S.M., Jautzy, J., Dietzel, M., 2021. Calibration of the dual clumped isotope thermometer for carbonates. Geochim. Cosmochim. Acta 312, 235–256.
Grossman, E.L., 2012. Applying Oxygen Isotope Paleothermometry in Deep Time. The Paleontological Society Papers 18, 9–68. https://doi.org/10.1017/S1089332600002540.
Grossman, E.L., Ku, T.-L., 1986. Oxygen and carbon isotope fractionation in biogenic aragonite: Temperature effects. Chem. Geol. 59, 59–74. https://doi.org/10.1016/0168-9622(86)90057-6.
Gunaskera, R.M., Patil, J.G., McEnnulty, F.R., Bax, N.J., 2005. Specific amplification of mt-COI gene of the invasive gastropod Maoricolpus roseus in planktonic samples reveals a free-living larval life-history stage. Mar. Freshw. Res. 56, 901–912.
Harris, I., Jones, P.D., Osborn, T.J., Lister, D.H., 2014. Updated high-resolution grids of monthly climatic observations - the CRU TS3.10 Dataset: Updataed high-resolution grids of monthly climate observations. Int. J. Climatol. 34, 623–642. https://doi.org/10.1002/joc.3711.
Harzhauser, M., Landau, B., 2019. Turritellidae (Gastropoda) of the Miocene Paratethys Sea with considerations about turritellid genera. Zootaxa 4681 (1), 1–136.
Huang, B., Thorne, P.W., et al., 2017. Extended reconstructed sea surface temperature version 5 (ERSSTv5), upgrades, validations, and intercomparisons. J. Clim. https://doi.org/10.1175/JCLI-D-16-0836.1.
Huntington, K.W., Petersen, S.V., 2023. Frontiers of carbonate clumped isotope thermometry. Annu. Rev. Earth Planet. Sci. 51, 611–641. https://doi.org/10.1146/annurev-earth-031621-085949.
Huyghe, D., Lartaud, F., Emmanuel, L., Merle, D., Renard, M., 2015. Palaeogene climate evolution in the Paris Basin from oxygen stable isotope (δ18O) compositions of marine molluscs. J. Geol. Soc. Lond. 172, 576–587. https://doi.org/10.1144/jgs2015-016.
Ivany, L.C., 2012. Reconstructing Paleoseasonality from Accretionary Skeletal Carbonates— Challenges and Opportunities: The Paleontological Society Papers, 18, pp. 133–166. https://doi.org/10.1017/S108933260000259X.
Ivany, L.C., Judd, E.J., 2022. Deciphering temperature seasonality in Earth's ancient oceans. Annu. Rev. Earth Planet. Sci. 50, 123–152.
Ivany, L.C., Lohmann, K.C., Hasiuk, F., Blake, D.B., Glass, A., Aronson, R.B., Moody, R. M., 2008. Eocene climate record of a high southern latitude continental shelf: Seymour Island, Antarctica. GSA Bull. 120 (5–6), 659–678. https://doi.org/10.1130/B26269.1.
Johnson, A.L.A., Valentine, A.M., Schöne, B.R., Leng, M.J., Sloane, H.J., Janeković, I., 2021. Growth-increment characteristics and isotopic (δ18O) temperature record of sub-thermocline Aequipecten opercularis (Mollusca:Bivalvia): evidence from modern Adriatic forms and an application to early Pliocene examples from eastern England. Palaeogeogr. Palaeoclimatol. Palaeoecol. 561, 110046. https://doi.org/10.1016/j.palaeo.2020.110046.
Jones, D.S., Allmon, W.D., 1995. Records of upwelling, seasonality and growth in stable-isotope profiles of Pliocene mollusk shells from Florida. Lethaia 28, 61–74. https://doi.org/10.1111/j.1502-3931.1995.tb01593.x.
Judd, E.J., Wilkinson, B.H., Ivany, L.C., 2018. The life and time of clams: Derivation of intra-annual growth rates from high-resolution oxygen isotope profiles. Palaeogeogr. Palaeoclimatol. Palaeoecol. 490, 70–83.
Kim, S.-T., O'Neil, J.R., Hillaire-Marcel, C., Mucci, A., 2007. Oxygen isotope fractionation between synthetic aragonite and water: Influence of temperature and Mg2+ concentration. Geochim. Cosmochim. Acta 71, 4704–4715. https://doi.org/10.1016/j.gca.2007.04.019.
Kwan, B.K.Y., Cheung, S.G., Alice, K.Y., Chan, P., Shin, K.S., 2018. Trophic and growth baseline of dominant subtidal gastropods in contrasting subtropical marine environments. Mar. Pollut. Bull. 127, 396–405. https://doi.org/10.1016/j.marpolbul.2017.12.033.
Lavín, M.F., Castro, R., Beier, E., Cabrera, C., Godínez, V.M., Amador-Buenrostro, A., 2014. Surface circulation in the Gulf of California in summer from surface drifters and satellite images (2004–2006). J. Geophys. Res. Oceans 119, 4278–4290. https://doi.org/10.1002/2013JC009345.
LeGrande, A.N., Schmidt, G.A., 2006. Global gridded data set of the oxygen isotopic composition in seawater. Geophys. Res. Lett. 33, L12604. https://doi.org/10.1029/2006GL026011.
Morton, B., Morton, J., 1983. The Sea Shore Ecology of Hong Kong, vol. 1. Hong Kong University Press.
Schmidt, G.A., Bigg, G.R., Rohling, E.J., 1999. Global Seawater Oxygen-18 Database v1.22. https://data.giss.nasa.gov/o18data/.
Scholz, S.R., Petersen, S.V., Escobar, J., Jaramillo, C., Hendy, A.J.W., Allmon, W.D., Curtis, J.H., Anderson, B.M., Hoyos, N., Restrepo, J.C., Perez, N., 2020. Isotope sclerochronology indicates enhanced seasonal precipitation in northern South America (Colombia) during the Mid-Miocene Climatic Optimum. Geology 48 (7), 668–672. https://doi.org/10.1130/G47235.1.
Scot, R.S., 1997. Aspects of the Biology of the Introduced Gastropod Maoricolpus Roseus. BSc Honors Thesis. Institute of Antarctic and Southern Ocean Studies, University of Tasmania, Hobart, 115 pp.
Shin, C., Allmon, W., Anderson, B., Kelly, B., Hiscock, K., Shin, P., 2020. Distribution and abundance of turritelline gastropods (Cerithioidea: Turritellidae) in Hong Kong and the English Channel: Implications for a characteristic fossil assemblage. J. Mar. Biol. Assoc. U. K. 100 (8), 1261–1270. https://doi.org/10.1017/S0025315420001204.
Shumway, S.E., 1979. The effects of fluctuating salinity on respiration in gastropod mollusks. Comp. Biochem. Physiol. 63, 279–283.
Surge, D., Lohmann, K.C., Dettman, D.L., 2001. Controls on isotopic chemistry of the American oyster, Crassostrea virginica : implications for growth patterns. Palaeogeogr. Palaeoclimatol. Palaeoecol. 172, 283–296. https://doi.org/10.1016/S0031-0182(01)00303-0.
Tao, K., Robbins, J.A., Grossman, E.L., O'Dea, A., 2013. Quantifying Upwelling and Freshening in Nearshore Tropical American Environments using Stable Isotopes in Modern Gastropods. Bull. Mar. Sci. 89, 815–835. https://doi.org/10.5343/bms.2012.1065.
Teusch, K.P., Jones, D.S., Allmon, W.D., 2002. Morphological Variation in Turritellid Gastropods from the Pleistocene to recent of Chile: Association with Upwelling Intensity. PALAIOS 17 (4), 366–377. https://doi.org/10.1669/0883135(2002)017<0366:MVITGF>2.0.CO;2.
Waite, R., Allmon, W.D., 2013. Observations on the Biology and Sclerochronology of Turritella leucostoma (Valenciennes, 1832; Cerithioidea: Turritellidae) from the Gulf of California. Am. Malacol. Bull. 31 (2), 297–310. https://doi.org/10.4003/006.031.0209.
Waite, R., Allmon, W.D., 2016. Observations on the biology and sclerochronology of "Turritella" Duplicata (Linnaeus, 1758) (Cerithioidea, Turritellidae) from Southern Thailand. Malacologia 59 (2), 247–269. https://doi.org/10.4002/040.059.0206.
Zhang, S.-R., Lu, X.X., Higgitt, D.L., Chen, C.-T.A., Sun, H.-G., Han, J.-T., 2007. Water chemistry of the Zhujiang (Pearl River): natural processes and anthropogenic influences. J. Geophys. Res. 112, F01011. https://doi.org/10.1029/2006JF000493.
Zhang, J.Z., Petersen, S.V., Winkelstern, I.Z., Lohmann, K.C., 2021. Seasonally variable aquifer discharge and cooler climate in Bermuda during the last interglacial revealed by subannual clumped isotope analysis. Paleoceanogr. Paleoclimatol. 36, e2020PA004145. https://doi.org/10.1029/2020PA004145.